Functional and Structural Development of Mouse Cone Photoreceptor Ribbon Synapses

Adam Davison, Kaspar Gierke, Johann Helmut Brandstätter, and Norbert Babai

Department of Biology, Animal Physiology/Neurobiology, Friedrich-Alexander-Universität Erlangen-Nürnberg, Staudtstrasse 5, Erlangen, Germany

Correspondence: Norbert Babai, Department of Biology, Animal Physiology/Neurobiology, Friedrich-Alexander-Universität Erlangen-Nürnberg, Staudtstr. 5, 91058 Erlangen, Germany; norbert.babai@fau.de.

Received: December 14, 2021
Accepted: March 2, 2022
Published: March 23, 2022

Citation: Davison A, Gierke K, Brandstätter JH, Babai N. Functional and structural development of mouse cone photoreceptor ribbon synapses. *Invest Ophthalmol Vis Sci.* 2022;63(3):21. https://doi.org/10.1167/iovs.63.3.21

Purpose. Cone photoreceptors of the retina use a sophisticated ribbon-containing synapse to convert light-dependent changes in membrane potential into release of synaptic vesicles (SVs). We aimed to study the functional and structural maturation of mouse cone photoreceptor ribbon synapses during postnatal development and to investigate the role of the synaptic ribbon in SV release.

Methods. We performed patch-clamp recordings from cone photoreceptors and their postsynaptic partners, the horizontal cells during postnatal retinal development to reveal the functional parameters of the synapses. To investigate the occurring structural changes, we applied immunocytochemistry and electron microscopy.

Results. We found that immature cone photoreceptor terminals were smaller, they had fewer active zones (AZs) and AZ-anchored synaptic ribbons, and they produced a smaller Ca^{2+} current than mature photoreceptors. The number of postsynaptic horizontal cell contacts to synaptic terminals increased with age. However, tonic and spontaneous SV release at synaptic terminals stayed similar during postnatal development. Multiquantal SV release was present in all age groups, but mature synapses produced larger multiquantal events than immature ones. Remarkably, at single AZs, tonic SV release was attenuated during maturation and showed an inverse relationship with the appearance of anchored synaptic ribbons.

Conclusions. Our developmental study suggests that the presence of synaptic ribbons at the AZs attenuates tonic SV release and amplifies multiquantal SV release. However, spontaneous SV release may not depend on the presence of synaptic ribbons or voltage-sensitive Ca^{2+} channels at the AZs.

Keywords: development, retina, cone photoreceptor, ribbon synapse, synaptic vesicle release

Photoreceptors continuously transduce light into graded membrane potential changes across a broad range of stimulus intensities.[1] A decrease in light intensity causes membrane depolarization and concomitant activation of voltage-sensitive Ca^{2+} channels, which in turn triggers the release of glutamate-filled synaptic vesicles (SVs).[2] In darkness, cone photoreceptors are constantly depolarized to approximately −40 mV, causing the high-frequency release of SVs. Exposure to light hyperpolarizes the photoreceptor membrane up to about −70 mV,[3,4] decreasing SV release. Therefore, SV release at photoreceptors could be categorized into tonic SV release in darkness when the voltage-sensitive Ca^{2+} channels are partially active and spontaneous SV release during light when the membrane potential sits far from the activation threshold of voltage-sensitive Ca^{2+} channels.

To ensure the supply of SVs for continuous release in response to fluctuating light stimuli, photoreceptors evolved a specialized release machinery, the ribbon-type synapse.[5,6] One of the unique properties of this synapse is the presence of the synaptic ribbon, an organelle anchored at the active zone (AZ), which tethers large numbers of SVs and consequently regulates the number of SVs present at the AZ. The elementary building block of synaptic ribbons is the protein ribeye.[7,8] However, other proteins also present at conventional synapses play a fundamental role in the organization and function of ribbon-type synapses.[9] Such proteins include bassoon, piccolo/piccolino, CAST, ELKS, and RIM.[10–13]

It is a well-accepted view that the main difference between ribbon-type and conventional synapses is the tonic SV release present at ribbon-type synapses, whereas neurotransmission at conventional synapses is strongly phase locked to presynaptic action potentials. However, the exact function of synaptic ribbons in SV release has not been identified, yet.

One of today's most commonly used animal models in visual neuroscience is the mouse. In mice, the development of photoreceptor ribbon synapses primarily occurs in the first 2 postnatal weeks.[14,15] During photoreceptor synaptogenesis, precursor spheres, which transport units that contain proteins of the presynaptic ribbon compartment like ribeye, bassoon, and piccolo/piccolino, arrive first at the nascent synapse.[16,17] Presynaptic proteins of the AZ compartment like Munc13, CAST, RIM, and the L-type Ca^{2+}

channel $\alpha 1$ subunit cluster directly at the AZ some time later.[16] At approximately postnatal day (P) 4, the transition from spherical ribbon material to elongated, free-floating synaptic ribbons and later on to anchored synaptic ribbons begins. Between P6 and P14, the percentage of elongated rod photoreceptor synaptic ribbons anchored to the AZ increases to near-adult levels,[16] which matches with the period in which postsynaptic horizontal cell (HC) and bipolar cell processes first contact photoreceptor terminals.[14,15] By the time of eye opening (P12–P13), development of the presynaptic machinery and assembly of postsynaptic structures is largely completed, and synaptic transmission is thought to be fully functional.

Unlike the existing knowledge about the structural development of photoreceptor ribbon synapses, we know very little about their functional development. So far, functional studies in mice are mainly based on electroretinographic recordings[18,19] and contradictory suction electrode recordings of rod photoreceptor light responses.[20,21] In the present study, we analyzed the functional development of ribbon synapses with patch–clamp recordings from cone photoreceptors and their postsynaptic HC partners in the mouse retina. We found that during postnatal development ribbon-free AZs are gradually occupied by synaptic ribbons, mimicking the transition from a ribbon-free synapse to a ribbon-type synapse, enabling us to learn more about the specific function of the ribbon in SV release by comparing SV release with parallel structural changes.

Methods

Animals

For these experiments, male and female C57BL/6 (Jackson Laboratories, Bar Harbor, ME) and Tg(Rac3-EGFP)JZ58Gsat/Mmcd (Rac3-EGFP) mice were used. Rac3–enhanced green fluorescent protein (EGFP) mice are of a C57BL/6 background and express EGFP in all cone photoreceptor cells. These were obtained from the Mutant Mouse Regional Resource Center, a National Center for Research Resources–National Institutes of Health–funded strain repository and were donated to the Mutant Mouse Regional Resource Center by the National Institute of Neurological Disorders and Stroke–funded GENSAT BAC transgenic project. Mice were kept on a 12-hour light/dark cycle. All experiments were performed in compliance with the guidelines for the welfare of experimental animals issued by the Federal Government of Germany, and the University of Erlangen-Nürnberg, and adhered to the ARVO Statement for the Use of Animals in Ophthalmic and Vision Research.

Slice Preparation and Electrophysiology

Horizontal retinal slice preparation was previously described in a video article.[22] Briefly, the mouse was anaesthetized with isoflurane (3%) and euthanized by cervical dislocation. The retina was removed from the eye and cut into pieces within Ames' media (Sigma-Aldrich, Munich, Germany). Then, the retina was mounted flat in 1.8% low melting agarose dissolved in Ames' medium and a horizontal cut (200 µm thick) was made through the inner nuclear layer using a vibratome (Leica Microsystems, Wetzlar, Germany). Vertical slices were prepared by cutting vertically oriented retina pieces. Slices were kept at 37 °C in an incubator containing 5% CO_2 and 50% O_2 for 20 to 30 minutes before recording.

Slices were visualized using a 63× water immersion objective (Zeiss, Jena, Germany) on a fixed stage microscope (Zeiss Axio Examiner). Whole cell currents were recorded using an EPC-10 patch-clamp amplifier (Heka Elektronik, Lambrecht, Germany), low-pass filtered at 2.9 kHz using a built-in Bessel filter, and digitized at 10 kHz with Patchmaster software (HEKA Elektronik GmbH, Reutlingen, Germany). All recordings were made at room temperature (22–24°C) under ambient light conditions. During recordings slices were perfused with bubbled (95% O_2/5% CO_2) extracellular solution containing (in mM/L^{-1}): 116 NaCl, 22.6 $NaHCO_3$, 1.25 NaH_2PO_4, 2.5 KCl, 2 $CaCl_2$, 1 $MgCl_2$, 10 glucose, 5 HEPES, 1 ascorbic acid, and 2 sodium pyruvate, adjusted to pH 7.4). Patch pipettes were pulled from borosilicate glass (Sutter Instruments, Novato, CA) to a final resistance of 5 to 7 MΩ for HC recordings and 10 to 14 MΩ for cone photoreceptor recordings.

For recording from HCs, slices were first perfused for 30 minutes in an extracellular solution containing 100 µM of the gap junction blocker meclofenamic acid.[27] Recordings of excitatory postsynaptic currents (EPSCs) were made using a potassium gluconate intracellular solution (in mM/L^{-1}): 136.6 K-gluconate, 5 EGTA, 13 TEA-Cl, 15 HEPES, 4 Mg-ATP, and 0.4 GTP (pH 7.2). HCs with a series resistance larger than 30 MΩ were excluded from analysis. Intracellular solution for I_{Ca} recording contained (in mM/L^{-1}): 136.6 Cs-gluconate, 5 EGTA, 13 TEA-Cl, 15 HEPES, 4 Mg-ATP, and 0.4 GTP (pH 7.2). For I_{AGlu} recordings, a hybrid cesium/potassium thiocyanate-based intracellular solution was used containing (in mM/L^{-1}): 82.5 potassium thiocyanate, 45.1 Cs-gluconate, 5 EGTA, 11 TEA-Cl, 11.6 HEPES, 3 Mg-ATP, 1.8 Na-GTP, 0.67 $CaCl_2$, and 0.67 $MgCl_2$ (pH 7.2).

EPSCs recorded from HCs, and I_{AGlu} events recorded from cone photoreceptors were analyzed using Mini Analysis software (Synaptosoft, Fort Lee, NJ). For the analysis, we collected 300 EPSCs and 100 I_{AGlu} events, respectively. To measure the I_{Ca} at the cone photoreceptor, a voltage ramp protocol was applied from −80 mV to +40 mV, with a speed of 0.1875 mV/ms. For the analysis of the current–voltage relationships evoked by the ramp protocol, the linear leak current was subtracted by fitting a line to the initial linear segment of the current trace (from −75 mV to −60 mV). The leak conductance was assumed to be ohmic. After leak subtraction, I_{Ca} traces were fitted with a Boltzmann function. The fitting region extended from the baseline to 5 mV beyond the peak inward current. Then, V_{50}, half-maximal activation of Ca^{2+} channels, and k the voltage dependence of Ca^{2+} channel activation was estimated.

Statistical Analysis

For normally distributed data a one-way ANOVA test was performed with the post hoc Tukey test for comparisons between individual groups. The assumption of normality was tested using the Shapiro–Wilk test and homogeneity of variances was tested using the Levenes test. Statistical testing in non-normally distributed data was performed using the Kruskal–Wallis test with post hoc pairwise Mann–Whitney U tests with adjustment of the P value for multiple comparisons using the Benjamini and Hochberg method. All data are presented as the mean ± standard error of the mean. For the analysis of the linear correlation between different parameters, the Pearson correlation coefficient was used.

Investigative Ophthalmology & Visual Science

Antibodies

The following primary antibodies where used for immunofluorescence staining: streptavidin–Cy3 conjugate (1:200, AAT Bioquest), rabbit anti-GFP (1:2000, Invitrogen, Darmstadt, Germany), guinea pig anti-GFP (1:1000, kind gift of Dr. Andreas Gießl), guinea pig Ribeye A-domain (1:10,000, Synaptic Systems, Göttingen, Germany), and rabbit α1f (1:3000, Synaptic Systems, Göttingen, Germany). The following secondary antibodies were used: guinea pig/rabbit Cy3 (Dianova, 1:300, Hamburg, Germany) and guinea pig/rabbit Alexa 488 (1:500, Molecular Probes, Eugene, OR).

Immunofluorescence Staining and Light Microscopy

Horizontal slices of the retinas were fixed for 10 minutes in 4% paraformaldehyde (PFA) and then incubated in blocking solution for 1 hour (0.5% triton-X 100). Primary antibody incubation was performed overnight, followed by secondary antibody incubation for 2 hours. For preparation of whole-mount retinas, the lens was removed from the eye and the eyecup was immersion fixed for 30 minutes in 4% PFA. After fixation, the retina was removed from the eyecup and washed with increasing concentrations of sucrose dissolved in 1× PBS (10%, 20%, and 30%) and subsequently subject to three freeze–thawing cycles using liquid nitrogen. Retinas were incubated in blocking solution for 1 hour. Primary antibody incubation was then performed for 24 hours, followed by secondary antibody incubation for 2 hours.

For quantification of labelled structures in cone photoreceptor terminals, image stacks of 0.1-µm sections of labelled cones terminals were captured using an LSM 710 laser scanning microscope (Carl Zeiss AG, Jena, Germany) equipped with a 63× (1.4 oil, Plan Apochromat) objective. Cone photoreceptor terminals were then 3D reconstructed in Imaris (BitPlane, Zurich, Switzerland), and ribbon or α1f labelling outside of the reconstructed cone terminal was subtracted. Labelled structures were manually analyzed in ImageJ (Rasband, W.S., ImageJ, US National Institutes of Health, Bethesda, MD). The length of ribbons was measured along the longest axis of the ribbon labelling using the Bezier curve tool in ImageJ. For quantification of the AZ area per cone photoreceptor terminal, α1f labelling was automatically thresholded using the otsu algorithm. For presentation, maximal intensity projections of cone photoreceptor terminals were generated and adjusted for contrast and brightness in ImageJ.

Individual HCs were loaded for 1 minute with a potassium gluconate based intracellular solution containing 1% neurobiotin tracer (Biozol, Eching, Germany) in horizontal slices of Rac3–EGFP mice. Slices were incubated for 30 minutes in Ames' solution containing 100 µM meclofenamic acid before cell loading, followed by anti-streptavidin–Cy3 conjugated antibody labelling. Samples were treated and imaged as described previously.

Electron Microscopy

For conventional electron microscopy, specimens were treated as described elsewhere, albeit with modifications.[11] Retinas of C56BL6/J mice at P6, P8, P10, and P30 were sequentially fixed in 4% PFA for 1 hour, followed by fixation in 2.5% glutaraldehyde for 2 hours at room temperature. Retinas were postfixed in 2% osmiumtetroxide and 3% $K_4[Fe(CN)_6]$ in 0.1 M cacodylate buffer for 1.5 hours. After dehydration in rising EtOH concentrations (30%–100%) and propylenoxide, retinas were embedded in Epon resin (Fluka, Buchs, Switzerland). For analysis, semithin sections were cut with an Ultracut E microtome (Reichert-Jung/Leica Biosystems, Nußloch, Germany). Finally, samples were contrasted with lead citrate and Uranyless (Delta Microscopies, Mauressac, France) in an automatic contrasting system (EM AC20, Leica Microsystems). Ultrathin sections were examined and photographed with an EM10 electron microscope (Carl Zeiss) equipped with a SC1000 OriusTM CCD camera (GATAN, Pleasanton, CA) in combination with the DigitalMicrograph 3.1 software (GATAN). For analysis, approximately 150 cone photoreceptor terminals per timepoint were photographed randomly and analyzed. Synaptic ribbons were classified according to their appearance as either free floating or attached.

Results

Synaptic Activity from Cone Photoreceptors Causes EPSCs at HCs Throughout Postnatal Development

To analyze the postnatal development of SV release rate from mouse cone photoreceptors, we performed whole cell patch-clamp recordings from postsynaptic HCs and measured EPSCs as a readout of presynaptic activity. Recordings were performed in horizontal retinal slices,[22] where the retina was cut through the inner nuclear layer to expose HCs whilst maintaining intact HC–photoreceptor contacts. HCs were identified by their relatively large size and the angular shape of their soma in the inner nuclear layer. Mouse retinal HCs belong to the B-type HCs, which possess a solitary long axon and a bushy dendritic arbor around the cell body.[23] HC dendrites receive input exclusively from cone photoreceptors, whereas their axon terminal contacts only rod photoreceptors.[24,25] Because the HC soma is connected by a several hundred micrometer long axon to its axon terminal, the dendritic and axonal arbor are considered to be electrically isolated.[26] Thus, EPSCs measured at the HC soma should reflect SV release only from cone photoreceptors. Moreover, we recorded EPSCs after 30 minutes of bath application of 100 µM meclofenamic acid to block gap junctions and thereby horizontal information flow in the retina.[27] All experiments were performed under ambient light conditions and HCs were held at −60 mV. We investigated synaptic development from P6 till adulthood. We considered mice older than 30 days (>P30) as adults, because at this time cone photoreceptor synapses are already developed fully.[15] For the developmental period from P6 to P13, we created groups with 2 days bin, because during this time major changes in synaptic morphology occur.[14,16] We observed SV release in all examined age groups, even before eye opening (Fig. 1A). The majority of the EPSCs showed complex waveforms, which were composed of multiple overlapping synaptic events (Fig. 1B). The mean frequency of synaptic events at the early phase of synapse development (P6–P7 and P8–P9) was significantly smaller than in the adult (>P30) group. By P10 to P11, the event frequency had already reached adult-like levels (approximately 400 Hz) (Fig. 1C). The mean amplitude of synaptic events did not change from P6 to adulthood (Fig. 1D). Moreover, we estimated the rate of SV release from cone photoreceptors by

Investigative Ophthalmology & Visual Science

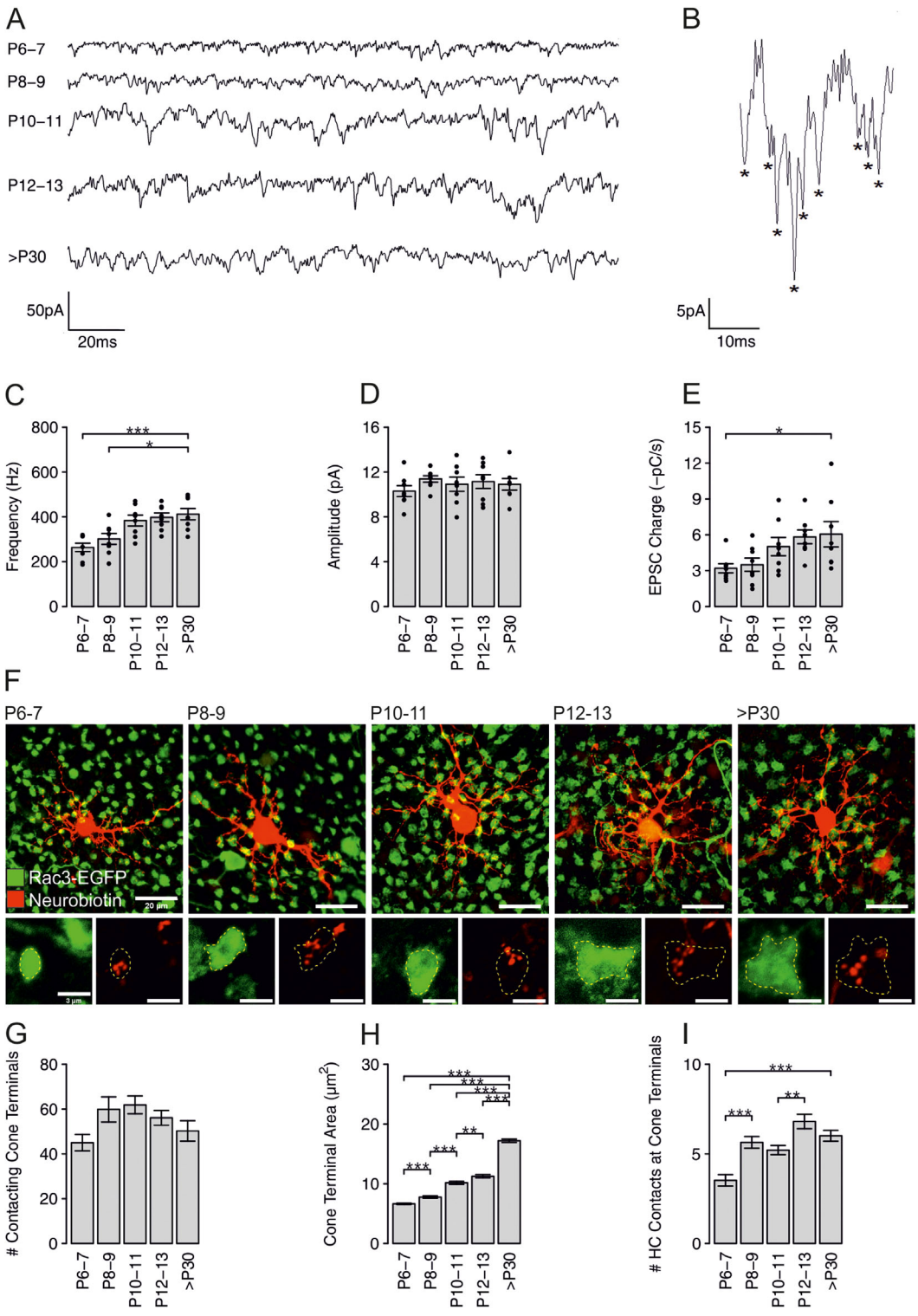

Figure 1. Postnatal changes in EPSCs recorded from HCs and in HC and cone photoreceptor synaptic terminal connectivity. (**A**) Representative EPSC traces at different developmental stages. HCs were held at a V_h of −60 mV. (**B**) Zoomed in view of tonic EPSCs recorded from a matured HC. Asterisks indicate EPSC events. (**C**) The mean frequency of tonic EPSCs. Significance was determined by one-way ANOVA test ($P < 0.001$, $n = 8$ cells). Tukey's multiple comparisons test (>P30 vs. P6–P7: $P < 0.001$, >P30 vs. P8–P9: $P = 0.01$). (**D**) Mean amplitude of tonic EPSCs. Significance was determined by one-way ANOVA test ($P = 0.953$, $n = 8$ cells). (**E**) The mean charge transfer rate of tonic EPSCs (−pC/s). Significance was determined by the Kruskal–Wallis test ($P = 0.0077$, $n = 8$ cells). Post hoc Mann–Whitney *U* test (>P30 vs. P6–P7: $P = 0.023$). (**F**) Immunofluorescence staining of horizontal retinal slices with labelling of individual HCs loaded with neurobiotin (*red*) and EGFP-labelled cone photoreceptor terminals (*green*). Dashed yellow lines outline cone photoreceptor terminals. (**G**) The mean number of contacting cone photoreceptor terminals per HC. Significance was determined by one-way ANOVA test ($P = 0.0695$, $n = 6$–9 cells). (**H**) The mean cone photoreceptor terminal area. Significance was determined by the Kruskal–Wallis test ($P < 0.001$, $n = 142$–149 terminals). Post hoc Mann–Whitney *U* test ($P < 0.001$ for all age groups vs. >P30, P6–P7 vs. P8–P9: $P < 0.001$, P8–P9 vs. P10–P11: $P < 0.001$, P10–P11 vs. P12–P13: $P = 0.0098$). (**I**) The mean number of HC contacts at cone photoreceptor terminals. Significance was determined by Kruskal-Wallis test ($P < 0.001$, $n = 51$–119 terminals). Post hoc Mann–Whitney *U* test (P6–P7 vs. P8–P 9: $P < 0.001$, >P30 vs. P6–P 7: $P < 0.001$, P10–P 11 vs. P12–P 13: $P = 0.0037$).

Investigative Ophthalmology & Visual Science

calculating the cumulative integral of EPSCs at postsynaptic HCs. Mean EPSC charge transfer values were only significantly different between the P6–P7 and the >P30 group (Fig. 1E, Table 1), indicating that the rate of SV release had already reached adult-like levels well before eye opening. At P10 to P11, EPSC charge had reached approximately 5 pC/s, which is close to the SV release rate measured in adults (approximately 6 pC/s). Using the measured average single event charge transfer value of 1.63 ± 0.054 fC (n = 51), we estimated the number of SVs released from cone photoreceptors. We found that the number of released SVs reaching HC dendrites almost doubles during development: approximately 1960 SVs/s (P6) and approximately 3708 SVs/s (>P30) (Table 1).

HC Connectivity to Cone Photoreceptor Terminals

HC somas distribute evenly in the inner nuclear layer close to the outer plexiform layer, where their dendrites contact numerous cone photoreceptor terminals.[3,28] Consequently, the measured EPSCs of HCs (Fig. 1A) should strongly depend on the number of contacting cone photoreceptor terminals. Thus, we counted how many cone photoreceptor terminals contact the dendrites of a single HC in each of the examined postnatal developmental stages. In horizontal retinal slices, HCs were neurobiotin-filled, subsequently fluorescently labelled, and their dendritic contacts to cone photoreceptor terminals were analyzed quantitatively. Cone photoreceptor terminals were visualized by using Rac3-EGFP reporter mice. This mouse strain expresses EGFP only in cone photoreceptors in the retina.[29,30] Individual HCs were contacted by numerous cone photoreceptors terminals in all examined age groups (Fig. 1F). We found that approximately 45 cone photoreceptor terminals contacted a single HC at P6 to P7. In adulthood, the number of contacting terminals showed an average value of approximately 50. Differences in the number of contacting terminals between developmental stages did not reach statistical significance (Fig. 1G, Table 2). A morphological analysis of cone photoreceptor terminals showed that their area progressively increased during postnatal development with an initial area of approximately 6.6 µm^2 at P6 to P7 and a final area of approximately 17.2 µm^2 at >P30 (Fig. 1H, Table 2). The number of postsynaptic HC dendritic contacts at single cone photoreceptor terminals also showed significant changes during postnatal development, with a significant increase in HC contacts between P6 and P9 and between P10 and P13 (Fig. 1I, Table 2). To estimate the SV release rate at a single cone photoreceptor terminal during postnatal development, we divided the measured SV release rate (Fig. 1E) by the number of contacting cone photoreceptor terminals (Fig. 1G). We found that SV release at a single cone photoreceptor terminal increased by 72% from P6 to >P30 (P6–P7: 43 SVs/terminal/s; >P30: 74 SVs/terminal/s) (Table 1).

Tonic SV Release at the Cone Photoreceptor Terminals During Postnatal Development

In the next set of experiments, we directly assessed tonic SV release from cone photoreceptor terminals during postnatal retinal development. We prepared vertical retinal slices from Rac3-EGFP mice at different postnatal ages and performed whole-cell patch-clamp recordings targeting the fluores-

Table 1. Physiological Synaptic Parameters During Postnatal Development

Age	P6–7	*n*	*N*	P8–9	*n*	*N*	P10–11	*n*	*N*	P12–13	*n*	*N*	>P30	*n*	*N*	*P* Value
Synaptic activity at HCs (–pC/s)	3.20 ± 0.38	8	2	3.50 ± 0.55	8	2	5.01 ± 0.76	8	3	5.82 ± 0.58	8	3	6.04 ± 1.07	8	5	0.0077 (Kruskal–Wallis)
Synaptic activity at HCs (vesicles/s)	1960 ± 241	8	2	2146 ± 345	8	2	3074 ± 476	8	3	3573 ± 371	8	3	3708 ± 663	8	5	–
I_{Aglu} in cones at −40 mV (–pC/s)	1.20 ± 0.20	6	3	1.38 ± 0.20	5	2	1.51 ± 0.21	8	4	1.50 ± 0.27	4	2	2.06 ± 0.26	8	3	0.1100 (ANOVA)
I_{Aglu} in cones at −40 mV (vesicles/s)	53.03 ± 9.46	6	3	60.84 ± 9.45	5	2	66.50 ± 10.08	8	4	65.93 ± 12.60	4	2	90.58 ± 12.43	8	3	–
% Multiquantal events	27.5 ± 5.03	6	3	39.6 ± 4.91	5	2	34.8 ± 6.72	8	4	32.5 ± 2.36	4	2	34.3 ± 6.24	8	3	0.768 (ANOVA)
Multiquantal event charge (–pC/s)	0.14 ± 0.02	6	3	0.11 ± 0.02	5	2	0.15 ± 0.04	8	4	0.17 ± 0.02	4	2	0.34 ± 0.03	8	3	0.001 (Kruskal–Wallis)
I_{Aglu} 10–90% rise time (ms)	2.76 ± 0.41	6	3	2.30 ± 0.20	5	2	2.83 ± 0.38	8	4	3.07 ± 0.60	4	2	2.98 ± 0.33	8	3	0.751 (ANOVA)
I_{Aglu} Tau decay (ms)	5.58 ± 0.71	6	3	4.98 ± 0.39	5	2	4.76 ± 0.73	8	4	4.78 ± 1.50	4	2	4.84 ± 0.59	8	3	0.645 (Kruskal–Wallis)
I_{Aglu} in cones at −65mV (–pC/s)	1.35 ± 0.25	6	3	1.19 ± 0.19	5	2	1.77 ± 0.40	8	4	2.01 ± 0.43	4	2	1.59 ± 0.14	8	3	0.503 (Kruskal–Wallis)
% Multiquantal Events	27.50 ± 3.99	6	3	31.80 ± 7.02	5	2	27.50 ± 2.97	8	4	39.00 ± 4.93	4	2	25.25 ± 4.25	8	3	0.350 (ANOVA)
Multiquantal event charge (–pC/s)	0.17 ± 0.04	6	3	0.17 ± 0.04	5	2	0.20 ± 0.01	8	4	0.18 ± 0.05	4	2	0.28 ± 0.05	8	3	0.403 (Kruskal–Wallis)
I_{Ca} Amplitude (pA)	−7.96 ± 1.60	5	3	−13.33 ± 1.19	11	3	−20.25 ± 2.05	7	2	−41.34 ± 6.30	8	3	−51.89 ± 6.67	12	4	<0.001 (Kruskal–Wallis)
I_{Ca} V_{50} (mV)	−48.94 ± 0.70	5	3	−38.45 ± 1.02	11	3	−37.95 ± 0.78	7	2	−38.23 ± 1.02	8	3	−32.52 ± 0.87	12	4	<0.001 (ANOVA)
I_{Ca} slope (pA/mV)	2.91 ± 0.30	5	3	7.77 ± 0.60	11	3	6.27 ± 0.86	7	2	5.04 ± 0.73	8	3	4.57 ± 0.30	12	4	<0.001 (Kruskal–Wallis)

* n denotes statistical n.
† N denotes animal n.

Table 2. Morphological Synaptic Parameters During Postnatal Development

Age	P6–7	n^*	$N^\dagger$	P8–9	n^*	$N^\dagger$	P10–11	n^*	$N^\dagger$	P12–13	n^*	$N^\dagger$	>P30	n^*	$N^\dagger$	*P* Value
No. of contacting cone terminals	45 ± 3.7	6	2	59.86 ± 5.6	7	3	61.88 ± 4.0	8	2	56.11 ± 3.3	9	3	50.25 ± 4.6	8	4	0.0695 (ANOVA)
Cone terminal area (μm^2)	6.64 ± 0.13	149	2	7.77 ± 0.20	144	3	10.16 ± 0.24	142	2	11.27 ± 0.28	146	3	17.21 ± 0.28	147	4	<0.001 (Kruskal–Wallis)
No. of HC contacts at cone terminals	3.53 ± 0.32	51	2	5.64 ± 0.32	104	3	5.21 ± 0.26	119	2	6.81 ± 0.40	84	3	6.01 ± 0.30	100	4	<0.001 (Kruskal–Wallis)
No. of AZs	4.34 ± 0.23	38	2	5.57 ± 0.34	30	2	8.65 ± 0.49	31	2	8.13 ± 0.48	32	2	13.52 ± 0.59	33	2	<0.001 (Kruskal–Wallis)
AZ area	1.06 ± 0.08	38	2	1.81 ± 0.14	30	2	2.43 ± 0.15	31	2	2.01 ± 0.13	32	2	4.47 ± 0.21	33	2	<0.001 (ANOVA)
No. of synaptic ribbons	5.29 ± 0.30	31	4	5.55 ± 0.30	31	3	7.30 ± 0.48	30	3	7.27 ± 0.62	29	3	10.65 ± 0.47	34	4	<0.001 (Kruskal–Wallis)
Synaptic ribbon length (μm)	0.62 ± 0.02	164	4	0.64 ± 0.02	172	3	0.82 ± 0.02	218	3	0.86 ± 0.02	218	3	1.04 ± 0.02	360	4	<0.001 Kruskal–Wallis)
% Attached synaptic ribbons	23.82 ± 4.45	4	4	23.90 ± 3.93	3	3	18.72 ± 1.40	3	3	32.78 ± 4.63	3	3	78.07 ± 2.77	4	4	<0.001 (ANOVA)

* n denotes statistical n.
† *N* denotes animal *n*.

cently (EGFP) labelled cone photoreceptors. The amplitude and frequency of tonic SV release were determined by measuring glutamate transporter anion currents (I_{AGlu}) at a −40 mV holding potential (V_h), a value that partially activates voltage-sensitive Ca^{2+} channels and triggers tonic SV release, mimicking dark-adapted conditions. In this condition, the ambient light under which recordings were performed would not influence the membrane potential because the cell is controlled by the current injected through the electrode. I_{AGlu} provides a trustworthy measure of exocytosis, reproducing the amplitude and frequency of released SVs.[31,32] To enhance I_{AGlu}, the patch electrode contained potassium thiocyanate. Tonic SV release was represented by simple and complex I_{AGlu} waveforms in all examined developmental stages (Figs. 2A–B). Individual synaptic events showed no change in rise and decay time from P6 to >P30 (Table 1), indicating that no different isoforms of glutamate transporters are present in young versus mature cone photoreceptors. Interestingly, we found large, recurring I_{AGlu} events in the majority of recordings in both developing and mature cone photoreceptors (P6–P7 = 4/6 cells, P8–P9 = 3/5 cells, P10–P11 = 4/8 cells, P12–P13 = 2/4 cells, >P30 = 4/8 cells) (Fig. 2C). In mature cone photoreceptors, these events had an average amplitude of 234.06 ± 49.04 pA and were characterized by a single rising phase and a decay phase consisting of two components (tau1 = 80.55 ± 6.73 ms, tau2 = 620.93 ± 272 ms). We did not measure the tonic SV release in recording sweeps containing recurring I_{AGlu} events because these currents were probably triggered by the sudden activation of ion channels other than L-type voltage-gated Ca^{2+} channels. The average frequency and amplitude of SV release were unchanged during postnatal development and stayed between approximately 25 and 30 Hz and approximately 4 pA, respectively (Figs. 2D–E). Although the cumulative amplitude distribution showed a larger proportion of high amplitude events at >P30 (Fig. 2F), the average charge transfer of I_{AGlu} events showed no significant change among the examined age groups even though values increased by 71% from P6 to >P30 (Fig. 2G, Table 1). The I_{AGlu} charge transfer of individual synaptic events was 22.71 ± 1.33 fC (n = 31). Accordingly, the calculated tonic SV release rate at developing cone photoreceptors was approximately 53 SVs/s (P6–P7) and approximately 91 SVs/s (>P30) (Table 1). These values are comparable with the SV release rates calculated using the EPSC measurements from HCs, indicating that glutamate receptor saturation does not influence the information transfer at the cone photoreceptor synapse during postnatal development. The larger proportion of high-amplitude synaptic events observed in the adult group (Fig. 2F) suggests the release of more than one SV simultaneously—multiquantal release. Therefore, we estimated the percentage of multiquantal synaptic events during tonic SV release. We classified synaptic events as multiquantal if their charge transfer was three times larger than that of a measured mean single synaptic event. We found that approximately 30% of the synaptic events were multiquantal from the early postnatal period till the adult stage (Table 1). However, multiquantal synaptic events of adult cone photoreceptors contained more SVs, shown by their significantly greater average charge transfer values (Fig. 2H, Table 1). P6 cone photoreceptors released on average approximately six SVs per multiquantal event, whereas >P30 cone photoreceptors released approximately 15 SVs. This finding indicates that the concomitant release of more than one SV

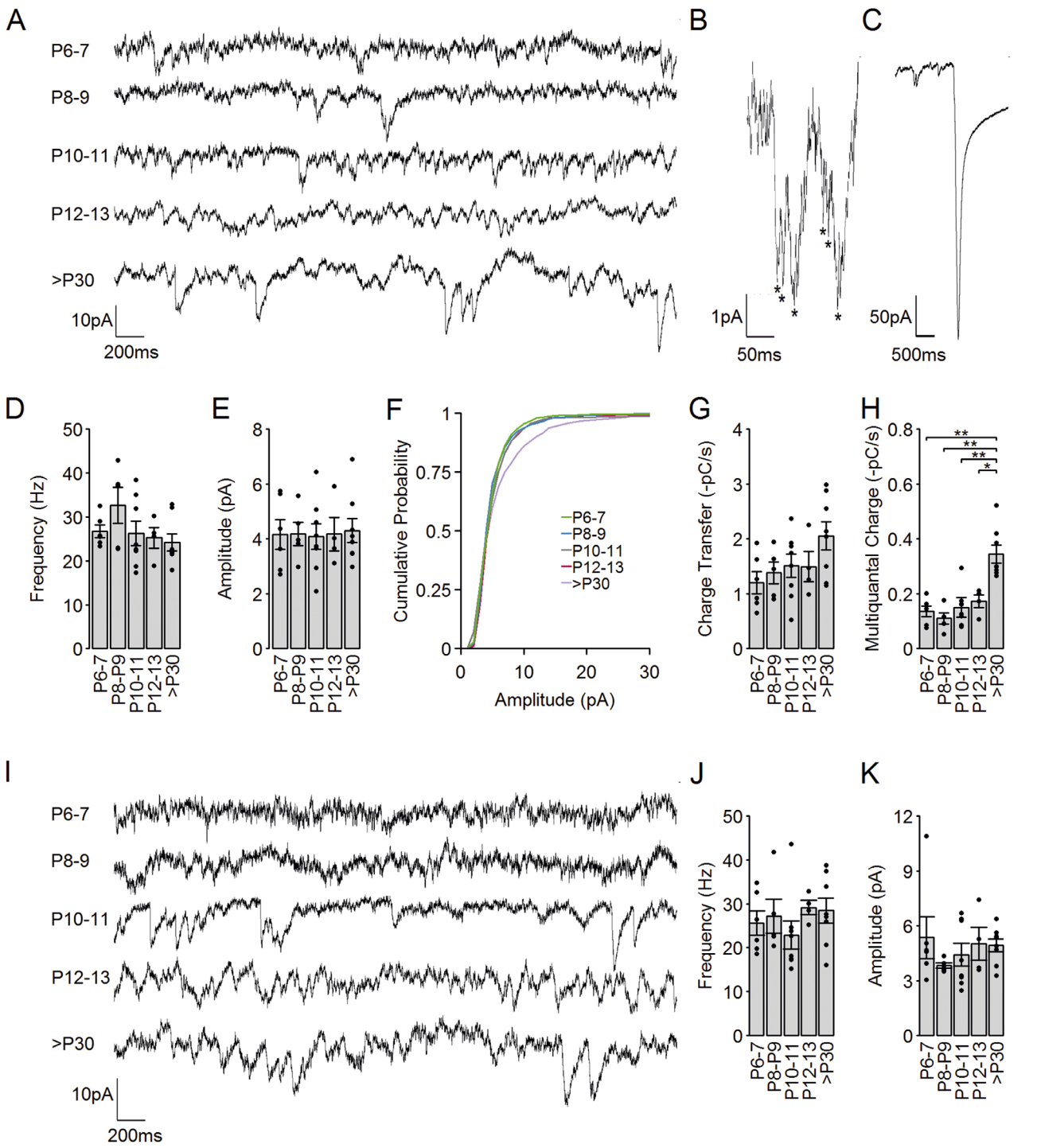

Figure 2. Postnatal changes in tonic and spontaneous vesicle release recorded from cone photoreceptors. (**A**) Representative traces of I_{AGlu} events recorded from developing cone photoreceptors held at a V_h of −40 mV. (**B**) Zoomed in view of I_{AGlu} events at >P30. Asterisks indicate synaptic events. (**C**) Representative trace of a recurrent, large amplitude I_{AGlu} event at >P30. (**D**) The mean frequency of events. Significance was determined by one-way ANOVA test ($P = 0.262$, $n = 4$–8 cells). (**E**) The mean amplitude of events. Significance was determined by one-way ANOVA test ($P = 0.998$, $n = 4$–8 cells). (**F**) Cumulative probability plot of the event amplitude (bin width = 1 pA). (**G**) The mean charge transfer rate of events. Significance was determined by one-way ANOVA test ($P = 0.110$, $n = 4$–8 cells). (**H**) The mean charge transfer of multiquantal events. Significance was determined by the Kruskal–Wallis test ($P = 0.001$, $n = 4$–8 cells). Post hoc Mann–Whitney U test (>P30 vs. P6–P7: $P = 0.0052$, >P30 vs. P8–P9: $P = 0.0052$, >P30 vs. P10–P11: $P = 0.0052$, >P30 vs. P12–P13: $P = 0.0101$). (**I**) Representative traces of I_{AGlu} events recorded from developing cone photoreceptors at a V_h of –65 mV. (**J**) The mean frequency of events. Significance was determined by the Kruskal–Wallis test ($P = 0.283$, $n = 4$–8 cells). (**K**) The mean amplitude of events. Significance was determined by the Kruskal–Wallis test ($P = 0.515$, $n = 4$–8 cells).

Investigative Ophthalmology & Visual Science

is occurring throughout the postnatal development of cone photoreceptor synapses.

Spontaneous SV Release at Cone Photoreceptor Terminals During Postnatal Development

Photoreceptors tonically release SVs at dark-adapted, depolarized membrane potentials when the voltage-sensitive Ca^{2+} channels are active. However, spontaneous SV release also exists at hyperpolarized membrane potentials.[33] Membrane hyperpolarization at adult photoreceptors is induced by the light activation of photopigments in the outer segments. The outer segments are not developed fully in the early postnatal stages and, consequently, photoreceptor activation by natural light stimuli is not possible.[14,34] Therefore, we hyperpolarized cone photoreceptors by voltage-clamping at a V_h of −65 mV and simultaneously measured I_{AGlu} as a read-out of spontaneous SV release (Fig. 2I). For the direct comparison of tonic and spontaneous release, we used the same cohort of cone photoreceptors as in Figures 2A–H. We found spontaneous SV release in all examined age groups, even before eye opening (Fig. 2I). The average frequency and amplitude of spontaneous synaptic events were not significantly different at the ages measured (Fig. 2J–K). Moreover, the charge transfer values, as a measure of the amount of spontaneous SV release, did not change significantly during cone photoreceptor postnatal development (Table 1). Furthermore, at a V_h of −65 mV, we did not detect the presence of the large amplitude, recurring I_{AGlu} events seen at a V_h of −40 mV, in any of the developmental stages measured, indicating that recurring I_{AGlu} events depend on membrane depolarization. Using the average charge transfer of spontaneous single synaptic events (24.61 ± 2.02 fC), we calculated the spontaneous SV release rates at cone photoreceptors in each developmental stage. Values showed 55 SVs/s at P6–P7 and 64 SVs/s at >P30 (Table 1). Interestingly, multiquantal SV release was present to a similar extent during the whole postnatal development (Table 1), and the number of SVs released during multiquantal events was also not significantly different (Table 1). These results suggest that the spontaneous release of SVs might occur independently from the development of cone photoreceptor synapses in the examined postnatal days.

Postnatal Development of Cone Photoreceptor Ca^{2+} Currents

The different types of neurotransmission, such as tonic and evoked, strongly depend on the activation of voltage-gated Ca^{2+} channels and therefore the influx of Ca^{2+} into the presynaptic terminal. Therefore, we measured Ca^{2+} currents (I_{Ca}) from developing cone photoreceptors using whole-cell patch-clamp recordings in vertical retinal slices of Rac3-EGFP mice (Fig. 3). To isolate I_{Ca} from K^+ currents, we used a standard TEA-Cl and cesium-containing intracellular solution, which has been used previously in mouse photoreceptors.[35] Photoreceptors were held at −60 mV. The relation between current amplitude and test potentials was tested by a voltage ramp protocol from −80 mV to +40 mV (0.1875 mV/ms). The typical leak subtracted I_{Ca} traces of cone photoreceptors are illustrated for the different age groups in Figure 3A. To characterize the developmental changes across age groups, we measured the peak I_{Ca} amplitude (Fig. 3B). Peak I_{Ca} showed a significant increase from −8 pA to −52 pA from P6 to >P30. Paired comparisons of the age groups showed a significant increase in peak I_{Ca} from P6 to P13 but not between P13 to >P30, indicating that peak I_{Ca} reached a value close to adult level already at P12 to P13 (Fig. 3B). The rising phase of the current voltage relationship could be fitted with a Boltzmann equation, which revealed the V_{50} (half activation kinetics) and k (slope factor). Interestingly, the V_{50} of voltage-gated Ca^{2+} channels measured at older age groups was more positive than in immature age groups (Fig. 3C), indicating that Ca^{2+} channel activation kinetics moved further away with age from the natural light stimulation evoked membrane potential change (approximately −40 mV in dark; approximately −70 mV in light). The slope factor showed a value of approximately 3 pA/mV in P6 to P7, which became approximately 8 pA/mV in P8 to P9 and showed a decrease to values close to approximately 5 pA/mV in >P30 (Fig. 3D). Smaller slope factor values indicate that Ca^{2+} channels produce a larger current response to a unit membrane potential change in their activation range.

Postnatal Development of Cone Photoreceptor AZs and Synaptic Ribbons

AZs are characterized by electron-dense structures that are firmly linked to the presynaptic plasma membrane. These regions are considered as release sites for SVs. As a marker of AZs at cone photoreceptor terminals, we stained whole-mount retinas of Rac3-EGFP mice for $Ca_v1.4$ voltage-sensitive Ca^{2+} channels, which are typically located in the nanometer range from the release-ready SVs at the AZ[2,36] (Fig. 4A). The morphological parameters of synaptic ribbons were measured in the same way staining whole-mount retinas of Rac3-EGFP mice with the synaptic ribbon marker ribeye (Fig. 4B). At an early postnatal stage, P6, AZ and ribeye staining in the cone photoreceptor terminals appeared as small puncta. As postnatal development progressed, punctate structures gradually changed to the typical horseshoe shape. Measurements of the stained structures are summarized in bar graphs (Figs. 4C–F). The number and area of AZs at cone photoreceptor terminals showed a significant increase from P6 to P10 and further between P12 and P30 (Figs. 4C–D; Table 2). The number of synaptic ribbons in cone photoreceptor terminals increased from approximately 5 (P6) to approximately 11 (P30) and their length from approximately 0.62 µm (P6) to approximately 1.04 µm (P30), respectively (Figs. 4E–F, Table 2).

In this analysis, we could not discriminate between free-floating and attached synaptic ribbons because of the insufficient resolution. Because the number of attached synaptic ribbons is an important factor for the release of SVs at the cone photoreceptor terminal, we next investigated ribbon synaptic development in cone photoreceptor terminals with electron microscopy. To follow the time course of ribbon attachment, we randomly photographed approximately 150 cone photoreceptor terminals for each age group and classified synaptic ribbons according to their appearance as either attached (Fig. 5A yellow arrowhead) or nonattached (Fig. 5A, red arrowhead). The relative abundance of anchored synaptic ribbons stayed low (approximately 20%–30%) until eye opening and then increased significantly until P30 with approximately 80% of the synaptic ribbons anchored to the AZ (Fig. 5B). This finding indicates that, in cone photoreceptors, ribbon anchoring primarily occurs after eye opening when light has full access to the retina.

Investigative Ophthalmology & Visual Science

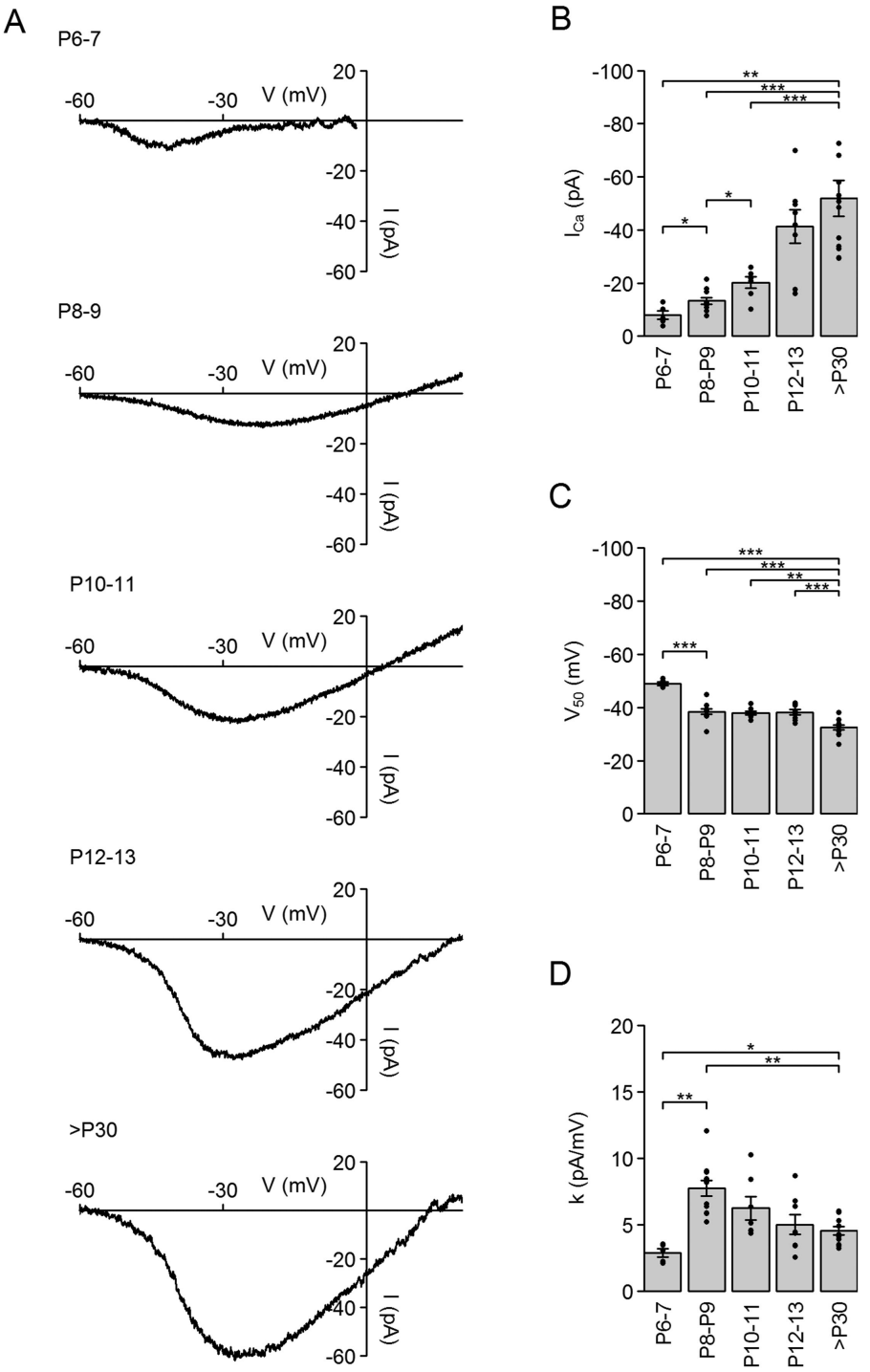

Figure 3. Postnatal changes in cone photoreceptor I_{Ca}. (**A**) Example cone photoreceptor I_{Ca} at the different developmental stages during a voltage ramp protocol from −80 mV to +40 mV, with a speed of 0.1875 mV/ms. (**B**) The mean amplitude of I_{Ca}. Significance was determined by the Kruskal–Wallis test ($P < 0.001$, $n = 5$–12 cells). Post hoc Mann–Whitney U tests (>P30 vs. P6–P7: $P = 0.0011$, >P30 vs. P8–P9: $P < 0.001$, >P30 vs. P10–P11: $P < 0.001$, P6–P7 vs. P8–P9: $P = 0.0475$, P8–P9 vs. P10–P11: $P = 0.0292$). (**C**) The mean half-maximal activation of the I_{Ca} (V_{50}). Significance was determined by the one-way ANOVA test ($P < 0.001$, $n = 5$–12 cells). Tukey's test for multiple comparisons (P6–P7 vs. P8–P9: $P < 0.001$, >P30 vs. P6–P7: $P < 0.001$, >P30 vs. P8–P9: $P < 0.001$, >P30 vs. P10–P11: $P = 0.0024$, >P30 vs. P12–P13: $P < 0.001$). (**D**) The mean I_{Ca} slope. Significance was determined by the Kruskal–Wallis test ($P < 0.001$, $n = 5$–12 cells). Post hoc Mann–Whitney U tests (P6–P7 vs. P8–P9: $P = 0.0032$, >P30 vs. P6–P7: $P = 0.0244$, >P30 vs. P8–P9: $P = 0.0032$).

Investigative Ophthalmology & Visual Science

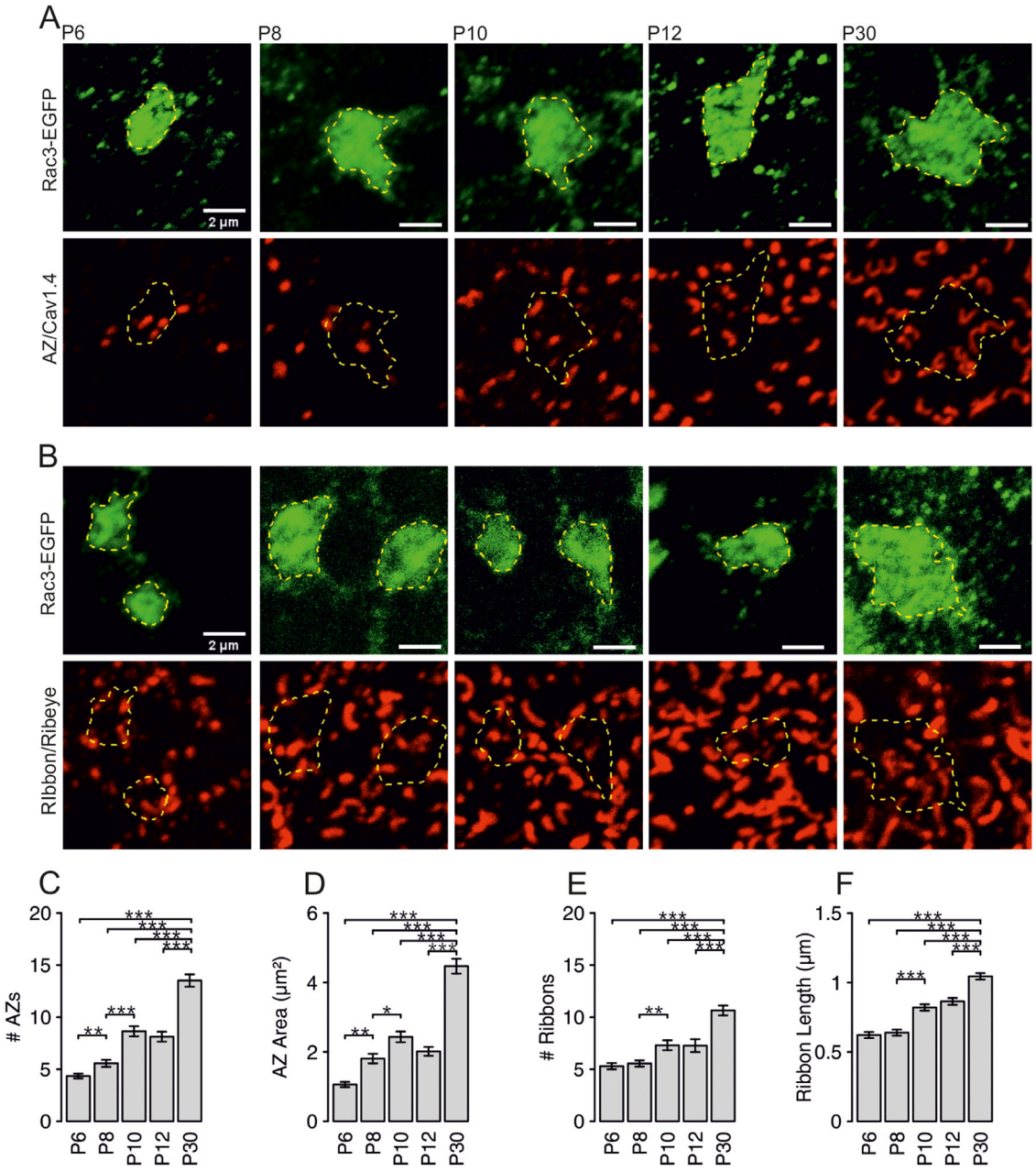

Figure 4. Postnatal changes in AZ and synaptic ribbon architecture in cone photoreceptor synaptic terminals. (**A, B**) Immunofluorescence staining of horizontal retinal slices, labelling for cone photoreceptor terminals (*green*) and (**A**) the α1f subunit of $Ca_v1.4$ voltage-gated Ca^{2+} channels (*red*) or (**B**) synaptic ribbons (ribeye A domain, *red*), at the different developmental stages. *Dashed yellow lines* represent the border of individual cone photoreceptor terminals. (**C**) The mean number of AZs. Significance was determined by the Kruskal–Wallis test ($P < 0.001$, $n = 30$–38 terminals). Post hoc Mann–Whitney *U* tests ($P < 0.001$ for P30 vs. all other age groups, P6 vs. P8, $P = 0.0056$, P8 vs. P10: $P < 0.001$). (**D**) The mean AZ area per cone photoreceptor terminal. Significance was determined by one-way ANOVA test ($P < 0.001$, $n = 30$–38 terminals). Tukey's tests for multiple comparisons ($P < 0.001$ for P30 vs. all other age groups, P6 vs. P8: $P = 0.004$, P8 vs. P10: $P = 0.044$). (**E**) Mean number of synaptic ribbons per cone photoreceptor terminal. Significance was determined by the Kruskal–Wallis test ($P < 0.001$, $n = 29$–34 terminals). Post hoc Mann–Whitney *U* tests ($P < 0.001$ for P30 vs. all other age groups, P8 vs. P10: $P = 0.0095$). (**F**) The mean length of the synaptic ribbons. Significance was determined by the Kruskal–Wallis test ($P < 0.001$, $n = 164$–360 ribbons). Post hoc Mann–Whitney *U* tests ($P < 0.001$ for P30 vs. all other age groups, P8 vs. P10: $P < 0.001$).

Relationship Between Ribbon Synapse Structure and SV Release

Finally, we examined the relationship between structural parameters, that is, the area of cone photoreceptor terminals, number of ribbons, area of AZs, and functional parameters, that is, tonic and spontaneous SV release, in developing cone photoreceptors (Fig. 6). We observed a linear correlation between the area of the cone photoreceptor terminal and (i) the number of synaptic ribbons present in the terminal, (ii) the amplitude of I_{Ca}, and (iii) the area of AZs (Figs. 6A–C) revealing a parallel postnatal development of the mentioned synaptic components (i, ii, iii). Furthermore, the number of AZs in a cone photoreceptor terminal

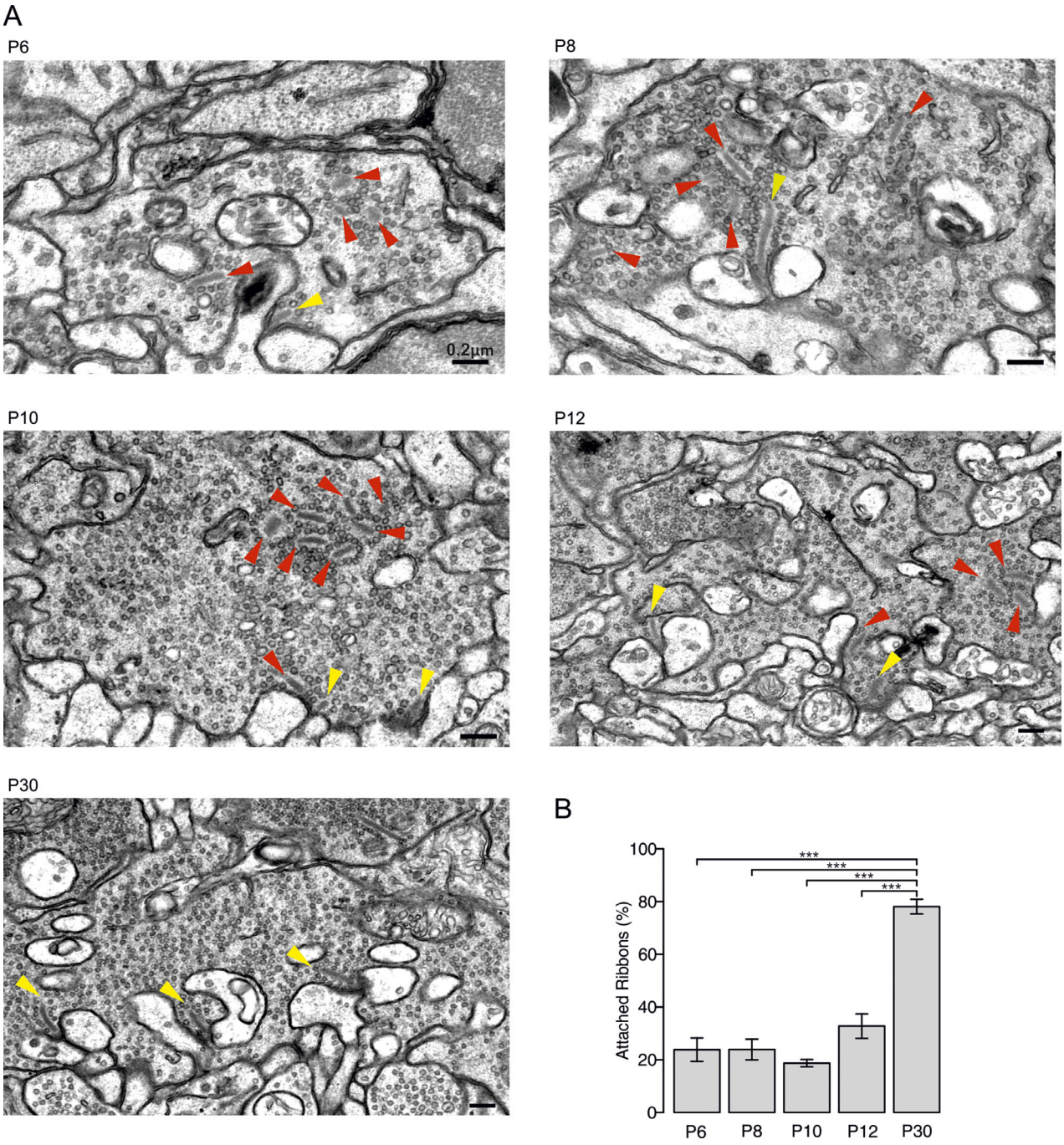

Figure 5. Ultrastructural analysis of synaptic ribbon development. (**A**) Representative electron micrographs of cone photoreceptor terminals at the different developmental stages. Yellow arrows indicate attached synaptic ribbons, red arrows indicate free-floating synaptic ribbons. (–) Mean percentage of attached synaptic ribbons. Significance was determined by one-way ANOVA test ($P < 0.001$, $n = 3$–4 animals). Post hoc Tukey's tests for multiple comparisons ($P < 0.001$ for P30 vs. all other age groups).

was linearly correlated with the amplitude of I_{Ca} (Fig. 6D), suggesting that Ca^{2+} channels localize at AZs in mature as well as in immature synaptic terminals. Tonic SV release directly measured from cone photoreceptors showed a linear correlation with I_{Ca} (Fig. 6E_1), but spontaneous SV release did not (Fig. 6F_1), which suggests that tonic, but not spontaneous, SV release seems to depend on Ca^{2+} levels. Moreover, tonic SV release from cone photoreceptors showed a linear correlation with the number of AZs (Fig. 6E_2), which was not the case for spontaneous SV release (Fig. 6F_2). To determine the effect of the presence of ribbons at AZs on SV release, we calculated the number of synaptic ribbons attached to AZs by multiplying the gross number of synaptic ribbons per cone photoreceptor terminals (Fig. 4E) with the percentage of synaptic ribbons attached to the AZ (Fig. 5B). Interestingly, we found a linear correlation between the number of AZ-attached ribbons and the number of vesicles released within multiquantal events during tonic SV release

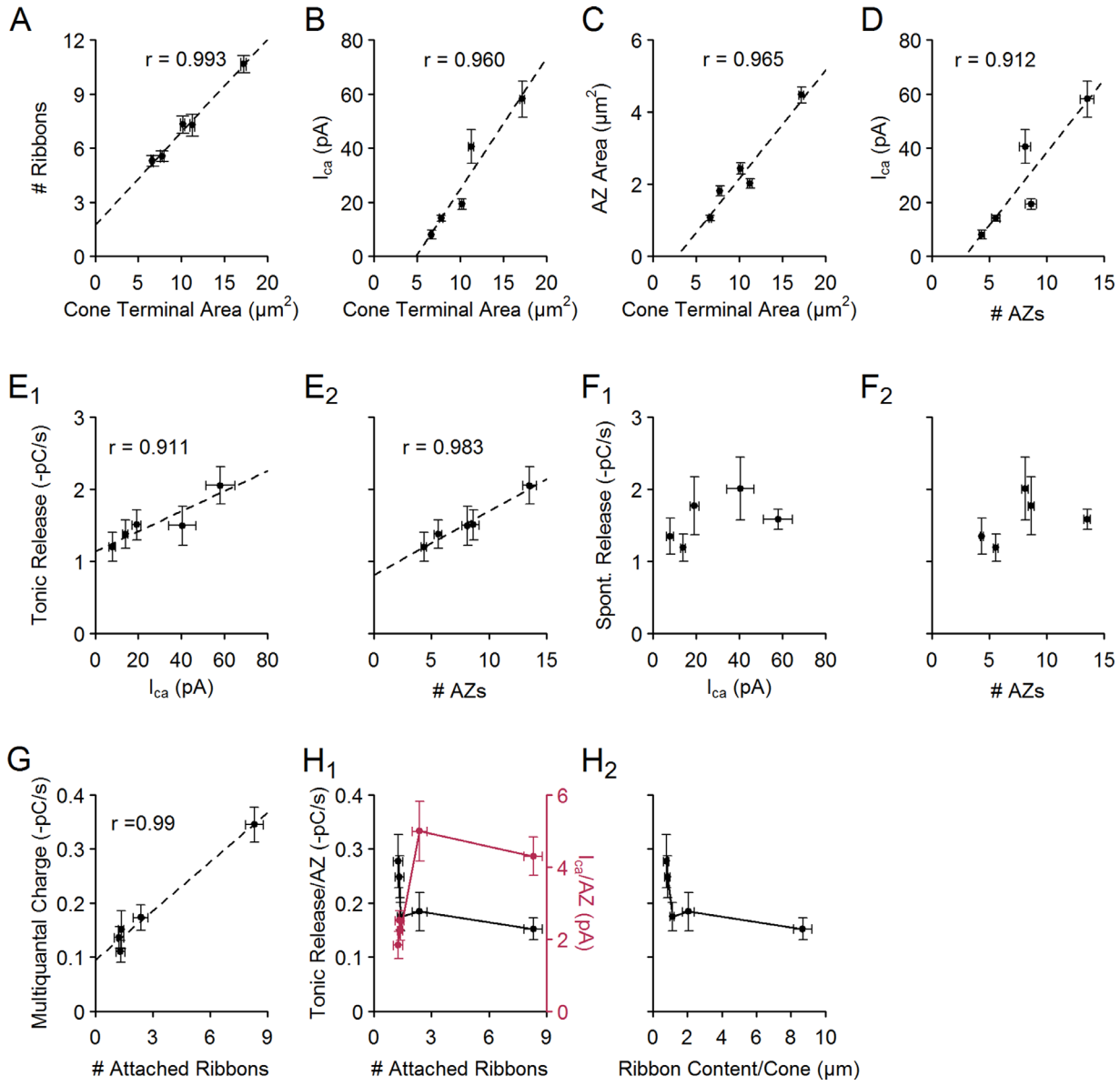

Figure 6. Correlations of the synaptic parameters during development. Data points are the measured synaptic parameters in the examined age groups (P6–P7, P8–P9, P10–P11, P12–P13, and >P30). The standard error of the mean of the *x* axis and *y* axis variables are included on all plots. All correlation tests were performed using the Pearson's correlation test. (**A–C**) Cone photoreceptor terminal area plotted against different synaptic parameters. Number of synaptic ribbons (**A**) ($P < 0.001$, r = 0.993), I_{Ca} (B, $P = 0.009$, r = 0.960), and AZ area per cone photoreceptor terminal (**C**) ($P = 0.008$, r = 0.965). (**D**) Plot of I_{Ca} against the number of AZs per cone photoreceptor terminal ($P = 0.0307$, r = 0.912). (**E_{1-2}**) Plot of tonic SV release per cone photoreceptor against different synaptic parameters. I_{Ca} (**E_1**) ($P = 0.032$, r = 0.911), number of AZs per cone photoreceptor terminal (**E_2**) ($P = 0.003$, r = 0.983). (**F_{1-2}**) Plot of spontaneous SV release per cone photoreceptor against different synaptic parameters. I_{Ca} (**F_1**) ($P = 0.377$, r = 0.512), number of AZs per cone photoreceptor terminal (**F_2**) ($P = 0.468$, r = 0.432). (**G**) Plot of multiquantal charge transfer against number of attached synaptic ribbons ($P = 0.00168$, r = 0.987). (**H_1**) Plot of number of attached synaptic ribbons per cone terminal against tonic SV release (*black*) and I_{Ca} amplitude per AZ (*red*). (**H_2**) Plot of tonic SV release against attached ribbon content per cone.

(Fig. 6G), suggesting that synaptic ribbons facilitate multiquantal release events. In contrast, we could not observe a clear relationship between spontaneous SV release and the number of ribbon-occupied AZs ($P = 0.841$ r = 0.125, Pearson's correlation test).

Next, we calculated the tonic SV release rate at single AZs by dividing the tonic SV release rate by the number of AZs. Tonic SV release at single AZs showed a negative relationship with the number of ribbon-occupied AZs (Fig. 6H_1, black trace). However, the I_{Ca} at single AZs showed a positive relationship with the number of AZ attached ribbons (Fig. 6H_1, red trace). This finding suggests that the appearance of synaptic ribbons at AZs of cone photoreceptor terminals decreases tonic synaptic activity. Finally, we estimated the ribbon content in cone photoreceptor terminals by multiplying the number of attached synaptic ribbons (Fig. 5B) with the average synaptic ribbon length (Fig. 4F). This parameter also showed a negative relationship with tonic SV

release (Fig. 6H$_2$), further supporting the hypothesis that the presence of synaptic ribbon decreases tonic synaptic activity at AZs of cone photoreceptor terminals.

Discussion

Synaptic ribbons were observed in photoreceptors more than 50 years ago.[37–39] So far, several studies have aimed to understand the functional and structural role of synaptic ribbon in SV release. In many of these studies, mouse lines were used that lack critical synaptic proteins such as bassoon (anchor of the ribbon to the AZ),[40–42] piccolino (structural organizer of the ribbon),[11] or ribeye (the building block of the ribbon).[43] However, in these mouse models, the mentioned synaptic proteins are absent or nonfunctional already at birth, which causes the structural reorganization of the synapse at the pre and postsynaptic sites[41,44] or an altered synaptic protein distribution.[43] Therefore, the observed functional phenotypes in synaptic transmission could also depend on the developmental reorganization of synapses. In contrast, we studied the functional and morphological changes of wild-type mouse cone photoreceptor ribbon synapses during postnatal development when the transition from ribbon-free to ribbon-occupied AZs occurs. These experiments provide additional insights into synaptic ribbon function.

Photoreceptor synaptic ribbons tether a large number of SVs in close proximity to the AZs, serving as a hotspot for SV release.[45] Therefore, the ribbon occupancy of AZs should strongly influence SV release during development. We found that the number of AZ-anchored synaptic ribbons stayed low (ribbon-free AZs = approximately 75%) from P6 until eye opening and then increased significantly up to P30 (ribbon-occupied AZs = approximately 80%). We asked the question of how this and other measured structural changes in the mouse cone photoreceptor synapse affected spontaneous and tonic SV release.

Interestingly, we found that SV release from mouse cone photoreceptors at a V_h of −65 mV (spontaneous release) was relatively steady during the examined postnatal period and might not be influenced by the increasing number of anchored ribbons and AZs. This finding suggests that spontaneous release might not happen necessarily at the AZ. Moreover, this finding is also consistent with the finding that the deletion of ribeye at retinal bipolar cells eliminated ribbons from the AZ and showed a major deficiency in Ca^{2+}-triggered SV release and in domain coupling of Ca^{2+} channels to release sites, but did not change spontaneous mEPSCs rates.[43] The Ca^{2+} dependence of spontaneous release was not expected; at a V_h of −65 mV, the voltage-sensitive Ca^{2+} channels are not active. The presence of relatively high spontaneous synaptic activity throughout the cone photoreceptors development is not unusual, because high spontaneous release rates have been reported in adult mice.[35] Nonetheless, the presence of spontaneous release after the eye-opening period is completely different from inner hair cell synapses, a ribbon-containing synapse in the cochlea, where the spontaneous activity ceases abruptly after hearing onset.[46] The high spontaneous activity in adult cone photoreceptors is probably necessary for the maintenance of synaptic connectivity, but may also be a hindrance because it decreases the signal-to-noise ratio of the synapse. Based on our measurements, we cannot tell why spontaneous release is persistent throughout postnatal development in cone photoreceptors, which could be a target for future research.

Earlier studies demonstrated the presence of $Ca_v1.4$ channels at the AZ in adult photoreceptors.[47,48] We found that $Ca_v1.4$ Ca^{2+} channels were present during the whole postnatal developmental period measured. This factor is likely to be critical for photoreceptor maturation because, without $Ca_v1.4$ channels, photoreceptor synapses have been found to stay immature in adulthood and are incapable of stabilization.[49,50] The measured linear correlation between the number of AZs and I_{Ca} amplitude and the increase of I_{Ca} amplitude itself likely reflects that voltage-sensitive Ca^{2+} channels are associated with AZs and that the number of expressed Ca^{2+} channels increases during development. Tonic SV release is triggered by the activation of voltage-sensitive Ca^{2+} channels. Our measurements suggest that tonic SV release at cone photoreceptor synapses is Ca^{2+} dependent and occurs at AZs during postnatal development. In contrast, the number of ribbon-occupied AZs showed a negative relationship with the rate of tonic SV release during postnatal development, suggesting that synaptic ribbons in cone photoreceptors may decrease the rate of tonic SV release. This hypothesis is supported by findings from studies that suggest that synaptic ribbons stabilize SVs at the AZ by acting as a trap or safety belt.[51] Nevertheless, evidence also exists that suggests that the synaptic ribbon is rather behaving like a conveyor belt and is involved in the coordination of vesicles to the AZ.[51] Our I_{AGlu} measurements also suggest that cone photoreceptor synaptic ribbons play a role in the coordination of tonic SV release, because we found that release events occurred more frequently in a form of multiquantal release when AZ-anchored ribbons were present. This finding is in agreement with experiments that have showed that synaptic ribbons are able to coordinate the synchronized fusion of multiple SVs.[52,53]

In general, photoreceptor synapses must be able to encode visual information continuously and, consequently, have a high demand for release-ready SVs, which requires the structural and functional specialization of the synaptic terminal. We found that several functional and structural synaptic parameters develop linearly during wild-type cone photoreceptor maturation. We used these relationships to make interpretations about the role of synaptic ribbons at the AZs in regard to tonic and spontaneous release of SVs. Up to now a defined model of ribbon function is still missing. Our results suggest that the synaptic ribbon is not involved in spontaneous SV release. Furthermore, the synaptic ribbon might control tonic SV release by decreasing the rate of SV release at the AZ, possibly creating a bigger reserve of release-ready, docked, and primed SVs for nonstop signaling and to support multiquantal SV release.

Acknowledgments

Supported by the Deutsche Forschungsgemeinschaft (DFG grant BA 6688/1-1). We thank Andrea Nerz and Katja Pertschy for excellent technical assistance.

Disclosure: **A. Davison,** None; **K. Gierke,** None; **J.H. Brandstätter,** None; **N. Babai,** None

References

1. Matthews G, Fuchs P. The diverse roles of ribbon synapses in sensory neurotransmission. *Nat Rev Neurosci*. 2010;11:812–822.

2. Bartoletti TM, Jackman SL, Babai N, Mercer AJ, Kramer RH, Thoreson WB. Release from the cone ribbon synapse under bright light conditions can be controlled by the opening of only a few Ca2+ channels. *J Neurophysiol*. 2011;106:2922–2935.
3. Feigenspan A, Babai N. Functional properties of spontaneous excitatory currents and encoding of light/dark transitions in horizontal cells of the mouse retina. *Eur J Neurosci*. 2015;42:2615–2632.
4. Korenbrot JI. Speed, sensitivity, and stability of the light response in rod and cone photoreceptors: facts and models. *Prog Retina Eye Res*. 2012;31:442–466.
5. Thoreson WB. Transmission at rod and cone ribbon synapses in the retina. *Pflug Arch Eur J Phy*. 2021;473:1469–1491.
6. Regus-Leidig H, Brandstatter JH. Structure and function of a complex sensory synapse. *Acta Physiol*. 2012;204:479–486.
7. Magupalli VG, Schwarz K, Alpadi K, Natarajan S, Seigel GM, Schmitz F. Multiple RIBEYE-RIBEYE interactions create a dynamic scaffold for the formation of synaptic ribbons. *J Neurosci*. 2008;28:7954–7967.
8. Schmitz F, Konigstorfer A, Sudhof TC. RIBEYE, a component of synaptic ribbons: a protein's journey through evolution provides insight into synaptic ribbon function. *Neuron*. 2000;28:857–872.
9. Schmitz F. The making of synaptic ribbons: how they are built and what they do. *Neuroscientist*. 2009;15:611–624.
10. Moser T, Grabner CP, Schmitz F. Sensory processing at ribbon synapses in the retina and the cochlea. *Physiol Rev*. 2020;100:103–144.
11. Muller TM, Gierke K, Joachimsthaler A, et al. A multiple Piccolino-RIBEYE interaction supports plate-shaped synaptic ribbons in retinal neurons. *J Neurosci*. 2019;39:2606–2619.
12. Hagiwara A, Kitahara Y, Grabner CP, et al. Cytomatrix proteins CAST and ELKS regulate retinal photoreceptor development and maintenance. *J Cell Biol*. 2018;217:3993–4006.
13. Lohner M, Babai N, Muller T, et al. Analysis of RIM expression and function at mouse photoreceptor ribbon synapses. *J Neurosci*. 2017;37:7848–7863.
14. Blanks JC, Adinolfi AM, Lolley RN. Synaptogenesis in the photoreceptor terminal of the mouse retina. *J Comp Neurol*. 1974;156:81–93.
15. Rich KA, Zhan Y, Blanks JC. Migration and synaptogenesis of cone photoreceptors in the developing mouse retina. *J Comp Neurol*. 1997;388:47–63.
16. Regus-Leidig H, Dieck ST, Specht D, Meyer L, Brandstatter JH. Early steps in the assembly of photoreceptor ribbon synapses in the mouse retina: the involvement of precursor spheres. *J Comp Neurol*. 2009;512:814–824.
17. Regus-Leidig H, Ott C, Lohner M, et al. Identification and immunocytochemical characterization of Piccolino, a novel Piccolo splice variant selectively expressed at sensory ribbon synapses of the eye and ear. *PloS One*. 2013;8:e70373.
18. Bakall B, Marmorstein LY, Hoppe G, Peachey NS, Wadelius C, Marmorstein AD. Expression and localization of bestrophin during normal mouse development. *Invest Ophth Vis Sci*. 2003;44:3622–3628.
19. Bonezzi PJ, Stabio ME, Renna JM. The Development of mid-wavelength photoresponsivity in the mouse retina. *Curr Eye Res*. 2018;43:666–673.
20. Luo DG, Yau KW. Rod sensitivity of neonatal mouse and rat. *J Gen Physiol*. 2005;126:263–269.
21. Ratto GM, Robinson DW, Yan B, McNaughton PA. Development of the light response in neonatal mammalian rods. *Nature*. 1991;351:654–657.
22. Feigenspan A, Babai NZ. Preparation of horizontal slices of adult mouse retina for electrophysiological studies. *Jove-J Vis Exp*. 2017;27:55173.
23. Peichl L, Gonzalez-Soriano J. Morphological types of horizontal cell in rodent retinae: a comparison of rat, mouse, gerbil, and guinea pig. *Vis Neurosci*. 1994;11:501–517.
24. Gallego A. Horizontal and amacrine cells in the mammal's retina. *Vision Res*. 1971;3(Suppl):33–50.
25. Kolb H. Organization of outer plexiform layer of primate retina - electron microscopy of Golgi-impregnated cells. *Philos T R Soc B*. 1970;258:261–+.
26. Nelson R, Lutzow AV, Kolb H, Gouras P. Horizontal cells in cat retina with independent dendritic systems. *Science*. 1975;189:137–139.
27. Veruki ML, Hartveit E. Meclofenamic acid blocks electrical synapses of retinal AII amacrine and on-cone bipolar cells. *J Neurophysiol*. 2009;101:2339–2347.
28. Reese BE, Raven MA, Stagg SB. Afferents and homotypic neighbors regulate horizontal cell morphology, connectivity, and retinal coverage. *J Neurosci*. 2005;25:2167–2175.
29. Fuchs M, Brandstatter JH, Regus-Leidig H. Evidence for a Clathrin-independent mode of endocytosis at a continuously active sensory synapse. *Front Cell Neurosci*. 2014;8:259.
30. Gong S, Zheng C, Doughty ML, et al. A gene expression atlas of the central nervous system based on bacterial artificial chromosomes. *Nature*. 2003;425:917–925.
31. Szmajda BA, DeVries SH. Glutamate spillover between mammalian cone photoreceptors. *J Neurosci*. 2011;31:13431–13441.
32. Hays CL, Sladek AL, Thoreson WB. Resting and stimulated mouse rod photoreceptors show distinct patterns of vesicle release at ribbon synapses. *J Gen Physiol*. 2020;152:e202012716.
33. Cork KM, Van Hook MJ, Thoreson WB. Mechanisms, pools, and sites of spontaneous vesicle release at synapses of rod and cone photoreceptors. *Eur J Neurosci*. 2016;44:2015–2027.
34. Olney JW. An electron microscopic study of synapse formation, receptor outer segment development, and other aspects of developing mouse retina. *Invest Ophthalmol*. 1968;7:250–268.
35. Grassmeyer JJ, Cahill AL, Hays CL, et al. Ca(2+) sensor synaptotagmin-1 mediates exocytosis in mammalian photoreceptors. *Elife*. 2019;8:e45946.
36. Dieck ST, Altrock WD, Kessels MM, et al. Molecular dissection of the photoreceptor ribbon synapse: physical interaction of Bassoon and RIBEYE is essential for the assembly of the ribbon complex. *J Cell Biol*. 2005;168:825–836.
37. Babel J, Simon G, Forgacs J, Englert U. [On the ultrastructure of the normal retina of the rabbit]. *Ber Zusammenkunft Dtsch Ophthalmol Ges*. 1966;67:146–150.
38. Goodland H. The ultrastructure of the inner plexiform layer of the retina of Cottus bubalis. *Exp Eye Res*. 1966;5:198–200.
39. Shiragami M. [Electron microscopic study on synapses of visual cells. IV. [The ultrastructure of synapses in the midperipheral area of chicken retina]. *Nihon Ganka Kiyo*. 1969;20:439–446.
40. Dick O, Dieck ST, Altrock WD, et al. The presynaptic active zone protein bassoon is essential for photoreceptor ribbon synapse formation in the retina. *Neuron*. 2003;37:775–786.
41. Babai N, Gierke K, Muller T, Regus-Leidig H, Brandstatter JH, Feigenspan A. Signal transmission at invaginating cone photoreceptor synaptic contacts following deletion of the presynaptic cytomatrix protein Bassoon in mouse retina. *Acta Physiol*. 2019;226:e13241.
42. Babai N, von Wittgenstein J, Gierke K, Brandstatter JH, Feigenspan A. The absence of functional bassoon at cone

Investigative Ophthalmology & Visual Science

photoreceptor ribbon synapses affects signal transmission at Off cone bipolar cell contacts in mouse retina. *Acta Physiol*. 2021;231:e13584.

43. Maxeiner S, Luo FJ, Tan A, Schmitz F, Sudhof TC. How to make a synaptic ribbon: RIBEYE deletion abolishes ribbons in retinal synapses and disrupts neurotransmitter release. *EMBO J*. 2016;35:1098–1114.
44. Regus-Leidig H, Fuchs M, Lohner M, et al. In vivo knockdown of Piccolino disrupts presynaptic ribbon morphology in mouse photoreceptor synapses. *Front Cell Neurosci*. 2014;8:259.
45. Zenisek D, Steyer JA, Transport Almers W., capture and exocytosis of single synaptic vesicles at active zones. *Nature*. 2000;406:849–854.
46. Tritsch NX, Bergles DE. Developmental regulation of spontaneous activity in the mammalian cochlea. *J Neurosci*. 2010;30:1539–1550.
47. Specht D, Wu SB, Turner P, et al. Effects of presynaptic mutations on a postsynaptic Cacna1s calcium channel colocalized with mGluR6 at mouse photoreceptor ribbon synapses. *Invest Ophthalmol Vis Sci*. 2009;50:505–515.
48. Morgans CW, Bayley PR, Oesch NW, Ren GY, Akileswaran L, Taylor WR. Photoreceptor calcium channels: insight from night blindness. *Vis Neurosci*. 2005;22:561–568.
49. Zabouri N, Haverkamp S. Calcium channel-dependent molecular maturation of photoreceptor synapses. *PloS One*. 2013;8:e63853.
50. Liu X, Kerov V, Haeseleer F, et al. Dysregulation of Ca(v)1.4 channels disrupts the maturation of photoreceptor synaptic ribbons in congenital stationary night blindness type 2. *Channels (Austin)*. 2013;7:514–523.
51. Parsons TD, Sterling P. Synaptic ribbon. Conveyor belt or safety belt? *Neuron*. 2003;37:379–382.
52. LoGiudice L, Matthews G. The role of ribbons at sensory synapses. *Neuroscientist*. 2009;15:380–391.
53. Singer JH, Lassova L, Vardi N, Diamond JS. Coordinated multivesicular release at a mammalian ribbon synapse. *Nat Neurosci*. 2004;7:826–833.

Investigative Ophthalmology & Visual Science